Retrieval of cloud droplet size from visible and microwave radiometric measurements during INDOEX: Implication to aerosols' indirect radiative effect

Guosheng Liu,[1] Hongfei Shao,[1] James A. Coakley Jr.,[2] Judith A. Curry,[3] Julie A. Haggerty,[4] and Mark A. Tschudi[4]

Received 15 October 2001; revised 18 February 2002; accepted 12 April 2002; published 3 January 2003.

[1] The effective radius of water cloud droplets is retrieved using remotely sensed passive microwave and visible data collected by aircraft during the Indian Ocean Experiment. The purpose of this study is to assess the aerosols' effect on cloud microphysical and radiative properties. To study this effect, we investigate the relationships among effective radius, liquid water path and number concentration of cloud droplets. The effective radius retrieval uses imager observations of reflected sunlight at 0.64 μm and liquid water path derived from microwave measurements. Results of an error analysis show that retrieval error is the largest for thin clouds having small visible reflectances and small liquid water path. For this reason, only pixels with visible reflectances greater than 0.2 are used in our data analysis, so that the maximum RMS error in effective radius is limited to about 4 μm. The relation between liquid water path and effective radius is examined for four different latitudinal regions. Results show that for the same liquid water path, effective radii are significantly smaller in the north than in the south, in correspondence to the north-south gradient of aerosol concentration in this region. In situ aircraft observations reveal larger cloud droplet number concentrations in the north than in the south. The north-south gradient of these variables are consistent with the aerosols' effect on cloud microphysics, that is, higher aerosol concentration increases the number concentration of cloud droplets, which, in turn, reduces droplet sizes given the same liquid water path and cloud thickness. Results based on comparison between data collected from northern and southern hemispheres suggest that the increase in aerosol number concentration alters cloud droplet numbers and sizes while leaving liquid water contents approximately the same. *INDEX TERMS:* 0305 Atmospheric Composition and Structure: Aerosols and particles (0345, 4801); 0320 Atmospheric Composition and Structure: Cloud physics and chemistry; 3359 Meteorology and Atmospheric Dynamics: Radiative processes; 3360 Meteorology and Atmospheric Dynamics: Remote sensing; *KEYWORDS:* cloud effective radius, liquid water path, aerosol's indirect effect, Indian Ocean Experiment

Citation: Liu, G., H. Shao, J. A. Coakley Jr., J. A. Curry, J. A. Haggerty, and M. A. Tschudi, Retrieval of cloud droplet size from visible and microwave radiometric measurements during INDOEX: Implication to aerosols' indirect radioactive effect, *J. Geophys. Res.*, *108*(D1), 4006, doi:10.1029/2001JD001395, 2003.

1. Introduction

[2] The radiative effect of aerosols arises both from the direct effect, that is, the direct scattering and absorption of sunlight by particles [*Ramanathan et al.*, 2001a], and also from the indirect radiative effect, which arises from the effect of aerosols on cloud microphysical and radiative properties of the clouds [e.g., *Twomey et al.*, 1984; *Coakley et al.*, 1987; *Radke et al.*, 1989]. Motivated by increasing awareness of the importance of both anthropogenic and natural aerosols to the Earth's radiation budget, the Indian Ocean Experiment (INDOEX) was designed to quantitatively assess the effect of aerosols on radiation through measuring the radiation budget, aerosol concentration, and clouds over the Indian Ocean. The Indian Ocean region was selected for this experiment because during the winter monsoon (January–March) the region provides a nearly ideal natural laboratory for observing the aerosol radiative forcing. Polluted air flows off the Indian and Southeast Asian subcontinents in the northeasterly flow over the Bay of Bengal and the Arabian Sea. The contrast between the high rates of aerosol emission over the Indian subcontinent and the

[1]Department of Meteorology, Florida State University, Tallahassee, Florida, USA.
[2]College of Oceanic and Atmospheric Sciences, Oregon State University, Corvallis, Oregon, USA.
[3]Program in Atmospheric and Oceanic Sciences, University of Colorado, Boulder, Colorado, USA.
[4]Atmospheric Technology Division, National Center for Atmospheric Research, Boulder, Colorado, USA.

0148-0227/03/2001JD001395$09.00

low rates of emission near the Intertropical Convergence Zone (ITCZ) south of the subcontinent has been observed to give rise to strong gradients in aerosol concentrations [*Rhoads et al.*, 1997; *Jayaraman et al.*, 1998; *Ramanathan et al.*, 2001b], and is hypothesized to be associated with corresponding gradients in cloud microphysical and optical characteristics.

[3] To assess the aerosols' indirect effect on radiation, the focus of this study is to retrieve the effective radius of water cloud droplets from simultaneous measurements of microwave and visible radiation above the clouds, and examining whether aerosol concentration has played a role in determining cloud drop size. The effective radius (r_e) is defined as the ratio of the third and second moments of the particle size distribution, that is,

$$r_e = \frac{\int_0^\infty r^3 n(r) dr}{\int_0^\infty r^2 n(r) dr}, \tag{1}$$

where *n(r)* is the number concentration of particles with radius *r*. Studies on effective radius retrievals have been conducted by *Nakajima and King* [1990], *Nakajima et al.* [1991], *Minnis et al.* [1992], *Han et al.* [1994], *Nakajima et al.* [2001] and *Szczodrak et al.* [2001] using combination of visible and near-infrared measurements, and by *Zuidema and Hartmann* [1995], *Greenwald et al.* [1995], *Lin et al.* [1998a, 1998b] and *Masunaga et al.* [2002] using combined visible and microwave measurements. *Han et al.* [1994] found that the effective radii are generally smaller for continental water clouds than for marine water clouds, and smaller in the northern hemisphere than in southern hemisphere, implying a systematic reduction of particle size due to high aerosol concentration. *Minnis et al.* [1992] reported that the diurnal variation of cloud droplets size observed during the First International Satellite Cloud Climatology Project (ISCCP) Regional Experiment (FIRE) off the coast of California can be explained by the diurnally changing wind direction that brings polluted continental air in the afternoon and clean oceanic air in the morning.

[4] In a nonprecipitating cumulus cloud, liquid water path, effective radius and number concentration of cloud droplets are interrelated parameters. For clouds with the same liquid water path and cloud thickness, the cloud with lower drop number concentration has a larger average effective radius. On the other hand, both liquid water path and cloud droplet size also increase as clouds develop. Consequently, a smaller effective radius near cloud top may be a result of high number concentration of cloud droplets, but may also be due to the cloud being suppressed. The former reflects the effect of aerosols because they are the source of cloud condensation nuclei (CCN), while the latter is apparently related to atmospheric stability and the water vapor supply. Therefore, to assess the effect of aerosols on cloud microphysics it becomes necessary to examine both liquid water path and effective radius, not effective radius alone. The interrelation among variables that are related to effective radius was discussed by *Han et al.* [1998], who derived the following relation among the relative changes of effective radius (r_e), liquid water path (*LWP*), cloud drop number concentration (N_c), and cloud thickness (h):

$$\frac{\Delta LWP}{LWP} \approx 3\frac{\Delta r_e}{r_e} + \frac{\Delta N_c}{N_c} + \frac{\Delta h}{h}. \tag{2}$$

If we consider a subset of clouds that all have the same observed *LWP,* and we assume the cloud thickness for this subset being similar, that is, $\Delta LWP/LWP = 0$ and $\Delta h/h \sim 0$, the relation becomes

$$\frac{\Delta N_c}{N_c} \approx -3\frac{\Delta r_e}{r_e}. \tag{3}$$

In other words, under the common value of *LWP* and the assumption that the cloud thickness for these clouds is similar, we may examine the change in cloud number concentration using the observed change in effective radius. It is noted that the above assumption is equivalent to assuming that mean liquid water content keep constant while changes occur. Results based on in situ aircraft microphysical observations in this region are consistent with this assumption [*Heymsfield and McFarquhar*, 2001]. This relation can also be derived for ideal adiabatic clouds while assuming a constant liquid water path [*Brenguier et al.*, 2000].

[5] We use retrievals of *LWP* and r_e and in situ aircraft measurement of cloud drop number concentration to investigate the aerosols' effect. In a previous study [*Liu et al.*, 2001], liquid water path was retrieved for the INDOEX experiment using airborne microwave data. In this study, we focus on the retrieval of effective radius of the clouds observed in the INDOEX region, and analyze its relation with liquid water path.

2. Instrumentation and Data

[6] The Multichannel Radiometer (MCR) and Airborne Imaging Microwave Radiometer (AIMR) were deployed on the NSF/NCAR C-130 aircraft during the 1999 intensive observation period of INDOEX to measure upward radiations from above the cloud. Eighteen flights were conducted from 16 February to 25 March 1999. MCR and AIMR data were collected, processed, and archived by NCAR's Atmospheric Technology Division. Observations extend from 10°S to 10°N mostly between 70° and 75°E except for the region north of 5°N where there are also data to the west of 70°E. Remotely sensed radiances from the MCR and the AIMR are the primary data source for cloud effective radius and liquid water path retrievals.

[7] The MCR is a seven-channel scanning radiometer measuring radiances from 0.64 to 10.8 μm [*Curran et al.*, 1981]. We use only data from channel 1 (0.64 μm) in this study; other channels had not been processed for this study. The field of view of MCR is 0.4°, resulting in a footprint on the ground of about 35 m when the aircraft flies at a nominal altitude of 5 km. The MCR scans ±45° across nadir with a scan rate of 3.5 times per second. The most recent calibration of the MCR performed at Los Alamos National Laboratory was used to relate radiance and voltage count. The radiance at channel 1 is expected to be accurate within ±1.4 W m^{-2} sr^{-1} μm^{-1} [*Curran et al.*, 1981; *Tschudi and Laursen*, 2001].

[8] The AIMR is a dual-frequency, dual-polarization total power radiometer that measures radiances at 37 and 90 GHz [*Collins et al.*, 1996]. The field of view is 1° for 90 GHz and

2.8° for 37 GHz, resulting in about 90 m and 250 m footprints, respectively, when the aircraft flies at a nominal altitude of 5 km. The AIMR scans ±60° across nadir covering a larger area than the MCR although only data where the two instruments overlap are analyzed in this study.

[9] The retrieval algorithm for liquid water path has been described by *Liu et al.* [2001]. It is optimized for AIMR channels under the INDOEX atmospheric conditions. This algorithm takes into account the better sensitivity of 90 GHz for thin clouds and the better sensitivity of 37 GHz for thick clouds. Results of analyzing clear-sky scenes show that the retrievals have essentially no bias and a random error of $\sim$18 g m^{-2}.

[10] Although the MCR and AIMR were onboard the same aircraft, separate data processing techniques were used. The data processing techniques for each system use different assumptions to perform calculations of pixel coordinates. As a result, the coordinates of data points do not match well with each other between the two instruments. This mismatch can be easily noticed by examining the images of raw data. The following procedure is introduced in order to obtain the best collocation. First, all observations are divided into small "scenes" with flight duration no more than 5 min. Within each scene, correlation coefficient is calculated between liquid water path and 0.64 μm radiance, first based on the coordinates provided by the raw data sets, and then shifting the MCR coordinates in cross-scan and along-track directions by 20 m each time. This procedure continues until a clear maximum correlation is found, and the best collocation match is determined.

[11] Since the pixel size of AIMR is several times larger than that of MCR, a weighted average is used to combine several MCR pixels to match an AIMR pixel. For a given AIMR pixel, we first select the MCR pixels that have a distance between their center and the center of the AIMR pixel less than half of the pixel size at AIMR 37 GHz. The weight assigned to a selected MCR pixel decreases with the distance of its center to the center of the AIMR pixel following the function $\exp(-d^2/2\sigma^2)$, where d is the distance and σ is a constant and can be determined by letting the weight reduce to half when d increases from 0 to half of the pixel size at AIMR 37 GHz. The weights are then normalized so that the sum of the weights of all selected MCR pixels equals unity. This analysis procedure effectively creates visible reflectances having the same spatial resolution as the AIMR brightness temperatures and being collocated with the AIMR field of view.

[12] For the retrievals of liquid water path and effective radius, only the data collected when the aircraft was flying level over cloud top are usable. As mentioned above, data are divided into scenes of less than 5 min each for data collocation purpose. As will be discussed below, scenes were restricted to contain low-level cumulus clouds having horizontal scales >2 km. Of all the available data, thirty-five cloudy scenes were found that satisfied these conditions. The locations of the scenes are shown in Figure 1.

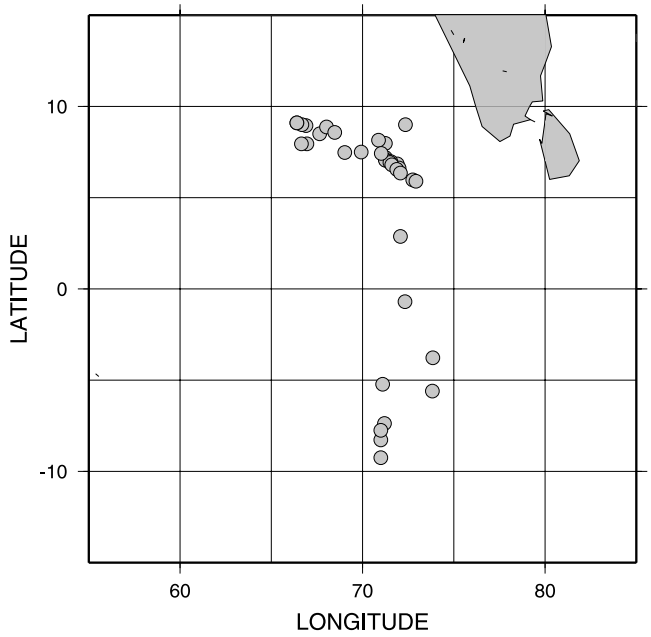

Figure 1. Locations of the thirty-five cloudy scenes analyzed in this study.

3. Cloud Effective Radius Retrieval

3.1. Description of the Retrieval Algorithm

[13] The effective radius retrieval is based on a lookup table generated in advance by a set of atmospheric radiative transfer simulations. The inputs for the lookup table are liquid water path retrieved from microwave data and visible reflectances at 0.64 μm defined by

$$R = \frac{\pi I_{obs}}{\mu_0 F_0}, \tag{4}$$

where I_{obs} is the observed radiance, μ_0 is the cosine of solar zenith angle and F_0 is the incident solar radiative flux at 0.64 μm. Apart from cloud microphysical properties, the reflected solar radiance also depends on solar zenith and azimuth angles, sensor viewing zenith and azimuth angles, and cloud altitude. In practice, many such lookup tables are produced, varying solar and sensor viewing angles by 5° and cloud top altitude by 0.5 km. Cloud base is assumed at 0.6 km, which is the typical convective condensation level in the region. Cloud top height is estimated from cloud top temperature measured by the nadir looking narrow band infrared radiometer onboard the C-130.

[14] The radiative transfer model used in the retrieval is the SBDART (Santa Barbara DISORT Atmospheric Radiative Transfer) model developed by *Ricchiazzi et al.* [1998]. This model is a combination of a discrete ordinate radiative transfer module [*Stamnes et al.*, 1988], low-resolution atmospheric transmission models, and Mie scattering formula for light scattering by water droplets and ice crystals. A modified gamma size distribution is used for cloud droplets:

$$n(r) = c\left(\frac{r}{r_e}\right)^{p-1} \exp\left(-\frac{p+2}{r_e}r\right), \tag{5}$$

where *n(r)* is the number concentration of cloud droplets with radius *r*, *c* is a normalization constant, *p* is a

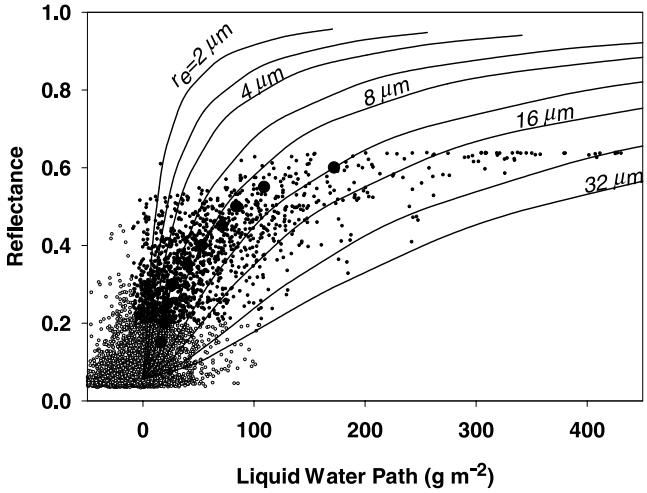

Figure 2. Relationship between liquid water path and reflectance (0.64 μm) calculated by a radiative transfer model for cloud effective radii from 2 to 32 μm (curves). The calculation is based on nadir observations at 0653 to 0658Z on 27 February 1999. Small open circles are all observational data at pixel level, small solid dots are those pixels that retrievals are applied, and large solid circles are the average of retrieved data at each 0.05 reflectance bin.

dimensionless parameter that controls the width of the distribution ($p = 7$ is used in the SBDART model). Detailed description of the model design and validation can be found in *Ricchiazzi et al.* [1998]. In the radiative calculations, a standard tropical atmosphere [*McClatchey et al.*, 1972] with 100% relative humidity in the cloud layer and a Lambertian ocean surface [*Tanre et al.*, 1990] are used. The ocean surface albedo at 0.64 μm is ~0.045. A standard maritime aerosol profile is used for all model runs. The aerosol optical depth at 0.64 μm for this profile is about 0.25. While the surface albedo and aerosol optical depth are taken to be constant throughout the INDOEX domain, the minimum cloud reflectance, 0.2, and optical depth, ~3, used in this study make the effects of varying surface albedo and aerosol optical depths negligible in this study. Because of the plane-parallel assumption, the three-dimensional effects are not included in the radiative transfer modeling, which constitutes a source of uncertainty in the effective radius retrieval, particularly for observations with large solar zenith angles.

[15] The basic concept underlying the determination of effective radius is illustrated in Figure 2. The figure shows the relationship between cloud liquid water path and 0.64 μm reflectances calculated with SBDART. Results are shown for effective radii from 2 to 32 μm and the reflectances were calculated at aircraft altitude. These relations were calculated based on nadir observations at 0653 to 0658Z on 27 February 1999, near 9°N and 66.5°E. Once *LWP* is determined from AIMR brightness temperatures, the corresponding 0.64 μm reflectance is used to determine the effective radius. This diagram shown in Figure 2 serves as a lookup table. Retrieved r_e are obtained through interpolation of the reflectances for a given *LWP*. Also shown in this figure are all available data points at pixel level (small open circles), data points for which retrievals were performed after screening (small solid circles), and the average of all retrievable points over each 0.05 interval in the 0.64 μm reflectance (large solid circles). On average, effective radii values for this case range from 6 to 12 μm while liquid water path values vary from 0 to 200 g m^{-2}. The reflectances shown in Figure 2 suggest that the MCR saturated when the reflected sunlight was large. Consequently, detailed analyses are restricted to clouds with liquid water paths less than about 200 g m^{-2}.

3.2. Error Analysis

[16] Since cloud drop effective radii are retrieved by the combination of microwave *LWP* and visible reflectances, we first examine the error characteristics of these two input variables. Due to the nonexistence of coincident validation data, the error characterization is done by analyzing the observed data for cloud-free regions. The frequency distribution of retrieved *LWP* for cloud-free regions is shown in Figure 3a, which indicates an almost zero mean and an 18 g m^{-2} standard deviation. That is, the systematic and random errors in the *LWP* retrieval are approximately 0 and 18 g m^{-2}, respectively. Similarly, we analyzed the difference between observed and radiative transfer model calculated

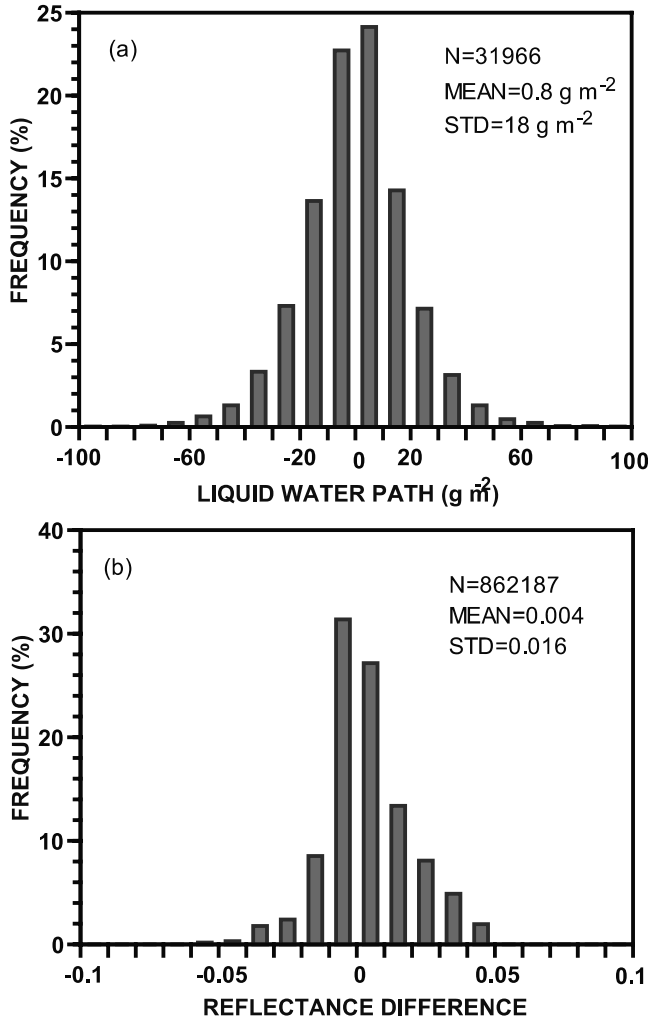

Figure 3. Error characteristics of (a) liquid water path and (b) reflectance derived from observations at clear-sky areas.

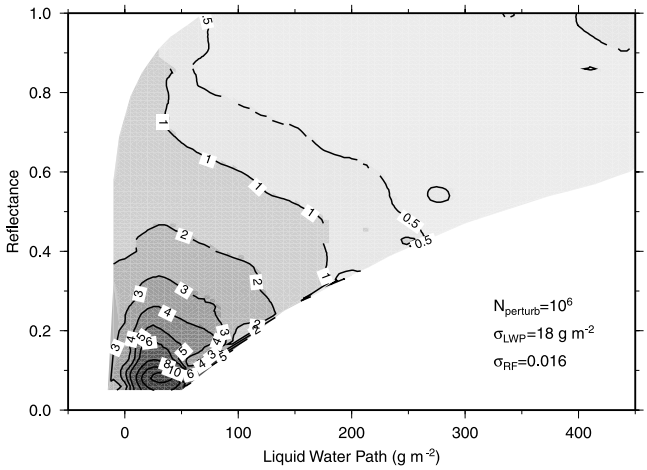

Figure 4. Root mean square error in effective radius retrievals estimated using a Monte Carlo procedure. Unit: μm. It is noted that the largest error occurs when both liquid water paths and visible reflectances are small.

reflectances for clear-sky regions (Figure 3b). The mean reflectance error is negligible and the standard deviation is 0.016, which is a measure of the random error. This error includes instrument noise and the uncertainties of variables used in the radiative transfer model, such as surface reflection, aerosol optical depth, etc.

[17] The random error in effective radii caused by the uncertainties in the input variables is then estimated by a Monte Carlo procedure. We randomly add noise to the input values within the range of plus and minus one standard deviation, that is, ±18 g m^{-2} for *LWP* and ±0.016 for reflectances, and compare the "retrieved" to the true (input) r_e. A similar procedure was used by *Liu and Curry* [2000] in analyzing random error in ice water path retrievals. Figure 4 shows the root mean square (*rms*) error after randomly perturbing the input variables for 10^6 times. The biggest error occurs when both *LWP* and reflectances are small (with the maximum error greater than 10 μm), and the RMS error decreases to less than 4 μm as *LWP* larger than 50 g m^{-2} or reflectances larger than 0.2. Clearly, the retrieval method is more suitable for relatively thick nonprecipitating clouds. Considering the large error associated with thin clouds, we use only pixels that have 0.64 μm reflectances greater than 0.2 regardless of viewing geometry in all the following discussions if not otherwise indicated, which limits the maximum RMS error in r_e to about 4 μm.

[18] Another important error that was not included in the above error analysis arises from the fact that clouds observed during INDOEX are boundary layer cumulus and have small horizontal scales, so that the plane-parallel assumption in our radiative transfer calculations is not strictly met. This error is very difficult to assess although it should decrease as the cloud's horizontal scale increases. For this reason, in our analysis we excluded the scenes that only have small clouds with horizontal scale less than 2 km.

[19] In Figure 5, we show one example of the retrievals. The images shown are liquid water path derived from microwave data (left), reflected visible radiance at 0.64 μm (middle) and retrieved effective radius (right) for 0653 to 0658Z on 27 February 1999, near 9°N and 66.5°E. The scene covers an area of approximately 12 km by 50 km and all available pixels including those with reflectance less than 0.2 are shown. The convective cells correspond well among the three images although the microwave *LWP* misses some small cells. The retrieved effective radius ranges from near zero to ~30 μm, with the largest value near the center of convective cells. Although there is no in situ measurement available to validate the r_e retrievals, the reasonable pattern shown here suggests that the algorithm can produce at least qualitatively correct results.

4. Results

4.1. A Clean Case and a Polluted Case

[20] We start the analysis by examining two cases observed in a clean and a polluted region, respectively. The first case was observed on 4 March 1999 near 9.3°S, 71.0°E (RF08), and the second case was observed on 27 February 1999 near 9°N, 66.5°E (RF06). The sizes of the cloud cells are comparable between the two cases. The averaged r_e for pixels with reflectance greater than 0.2 is about 15 and 10 μm for RF08 and RF06 case, respectively.

[21] Figure 6 shows the *LWP*-r_e relationship by frequency distribution for the two cases. The frequency is calculated by the pixel number within each 30 g m^{-2} *LWP*

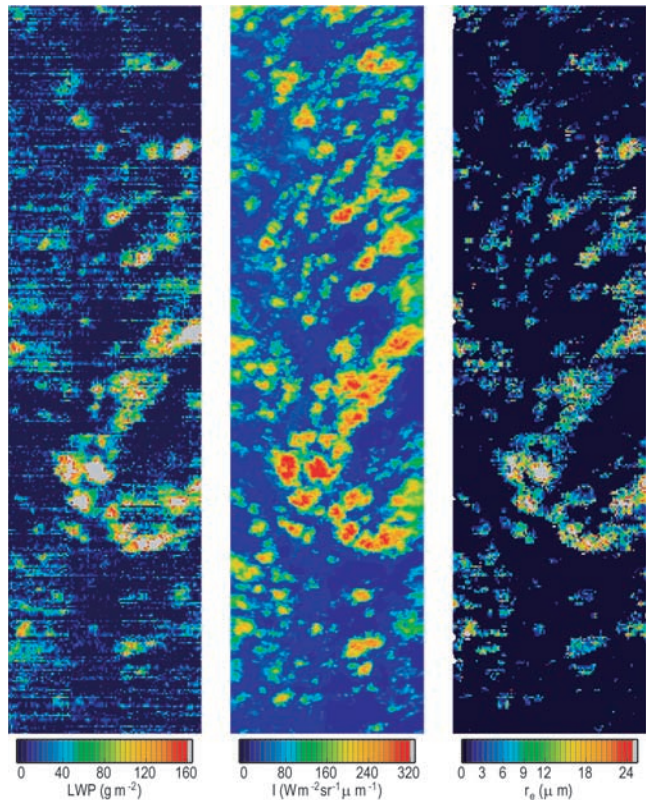

Figure 5. Images of liquid water path (left), reflected radiance at 0.64 μm (middle) and effective radius (right) for the cloudy scene of 0653 to 0658Z on 27 February 1999. The scene covers an area of approximately 12 km by 50 km.

and 3 μm r_e bin, which is then normalized by the total pixel number and multiplied by 1000. The general trend of the *LWP*-r_e relation is that r_e increases with *LWP*, which may be predicted by an adiabatic cloud model [e.g., *Brenguier et al.*, 2000]. In the figure, the solid dots show the modal effective radii that are determined by the maximum frequency at fixed liquid water path. Despite the scatter in the frequency distribution, we can still find the general trend by following the modal effective radius as *LWP* increases. From this trend, it is seen that r_e increases more sharply in the RF08 case than in the RF06 case. For example, the modal r_e increases from 3 to 20 μm as *LWP* changes from 0 to150 g m^{-2} in the RF08 case, while it only increases from 3 to 13 μm for the same *LWP* variation in the RF06 case.

[22] The difference in cloud microphysics between the two cases is further shown by the r_e frequency distributions at fixed liquid water path as shown in Figure 7. The frequency is normalized by the total pixel number at the given liquid water path bin (25 g m^{-2}) so that the integrated frequency for all effective radii is 100. Except for *LWP* = 25 g m^{-2}, the cloud in the clean case (RF08) shows systematically larger effective radii than the cloud in the polluted case (RF06). The difference in modal effective radii between the two cases exceeds 5 μm for *LWP* of 100 and 150 g m^{-2}. In other words, for the same value of *LWP*, clouds in the RF06 case are more likely to contain smaller water droplets than clouds in the RF08 case. As mentioned earlier, the northern region is polluted and thus contains more aerosols. The smaller droplet size may be interpreted as a result of the high number concentration of CCN.

[23] Limited particle number concentration data were collected by the Forward Scattering Spectrometer Probe 100 (FSSP-100) and 300 (FSSP-300) [*Dye and Baumgardner*, 1984]. The FSSP-100 measures cloud particles ranging from 2 to 47 μm while the FSSP-300 measures particles ranging from 0.3 to 20 μm, both with a precision of 16% for number concentration. The number concentration obtained from the FSSP-100 and FSSP-300 is plotted in Figure 8, corresponding to the two cases. Note that the FSSP data are not necessarily sampled from the same clouds as those shown for Figure 6 and 7. Our assumption is that the number concentrations of any clouds in the same area are similar except near the cloud edges where the cloud water is diluted by mixing with surrounding drier air. In the RF08 case, the aircraft sampling was conducted near the cloud base of 550 m altitude while the sampling was done through the layer between 700 and 1300 m in the RF06 case. For nondrizzling boundary layer cumulus clouds, cloud drop concentration does not vary much throughout the cloud's vertical extent. In other words, the value sampled near cloud base in the RF08 case also reflects the cloud drop concentration throughout the entire cloud. It is also reasonable to consider that the maximum values in the number concentration profiles reflect the droplet concentration where the cloud water has not been diluted by dry air. Therefore, it appears that there is a significant difference in cloud droplet number concentrations between clouds in the two cases. For example, the maximum value of FSSP-100 counts is ~100 cm^{-3} in the RF08 case while it is ~400 cm^{-3} in the RF06 case. Recalling that the southern region (RF08) is far from the pollution source of Indian subcontinent, the difference between the two cases is a strong indication of the aerosols' effect on cloud microphysics.

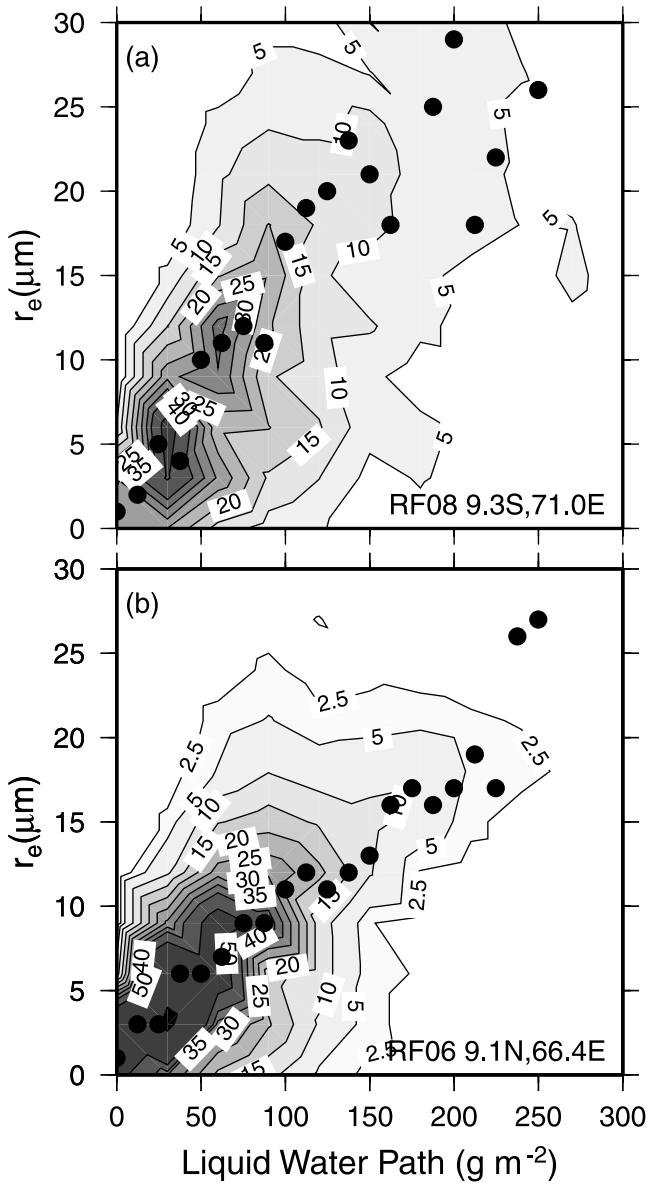

Figure 6. Frequency distribution of pixel occurrence in the two-dimensional diagram of liquid water path and effective radius for (a) the clean case on 4 March 1999 (RF08) near 9.3°S, 71.0°E and (b) the polluted case on 27 February 1999 (RF06) near 9.0°N, 66.5°E. Solid dots show the modal effective radii at fixed liquid water path.

4.2. Relationship Between *LWP* and r_e Observed During INDOEX

[24] Using data from the 35 scenes shown in Figure 1, the averaged *LWP* and r_e values are calculated for each 5°-latitude region. Note that there is only one scene in the 0–5°N region and two scenes in the 0–5°S region. The latitudinal distribution and scatterplot (inset) of *LWP* and r_e are shown in Figure 9. Only pixels with reflectance greater than 0.2 are included in the averaging. The clouds

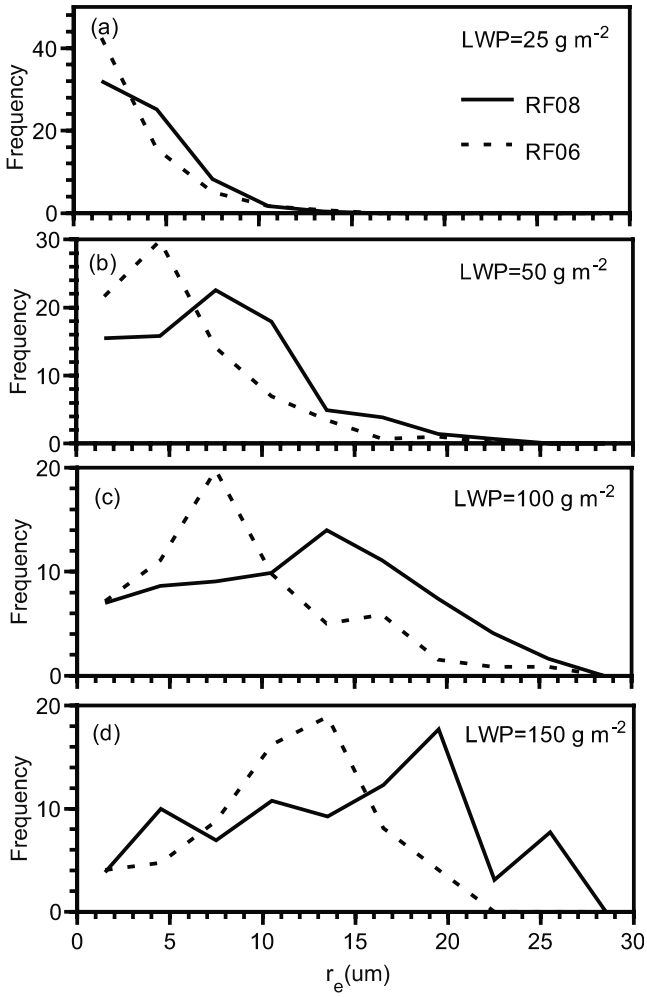

Figure 7. Comparison of frequency distributions of effective radius at liquid water path of (a) 25 g m^{-2}, (b) 50 g m^{-2}, (c) 100 g m^{-2}, and (d) 150 g m^{-2} between the clean case (RF08) and the polluted case (RF06).

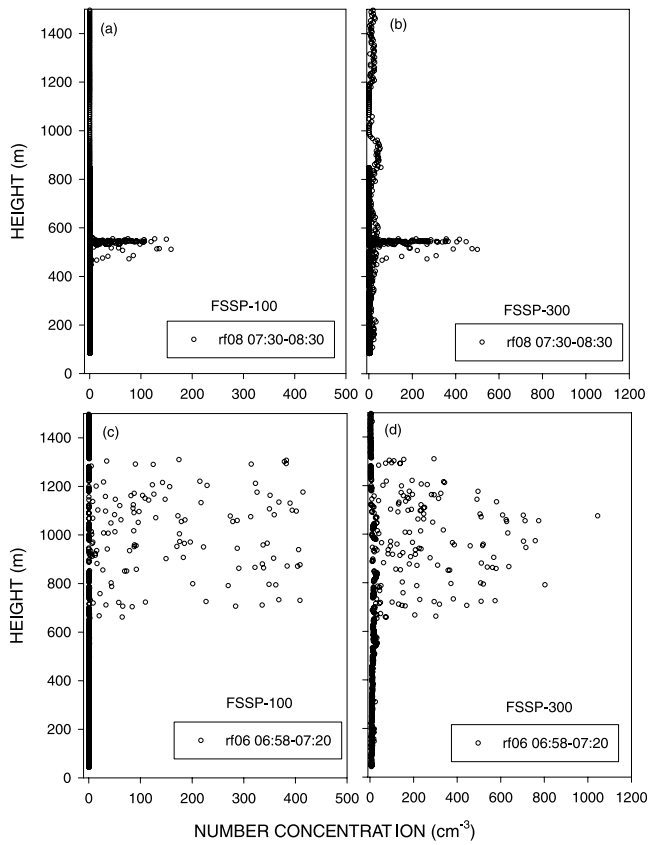

Figure 8. Particle number concentrations measured by FSSP-100 and FSSP-300 probes for (a–b) the clean case and (c–d) the polluted case.

observed in the southern part of the domain both have greater *LWP* and larger r_e than those observed in the north. The scatterplot shows the positive correlation between *LWP* and r_e.

[25] The frequency distributions of the *LWP*-r_e relation for the 4 latitudinal regions are shown in Figure 10, which are calculated using the same procedure as that for the case studies previously discussed. The solid dots, showing the modal effective radii at fixed *LWP*, illustrate the general trend of the *LWP*-r_e relation. For *LWP* value of 100 g m^{-2}, the most probable r_e is around 10 μm in the northern regions while larger than 15 μm in the southernmost region.

[26] To further illustrate the latitudinal difference, we calculated the frequency distribution of effective radii at fixed *LWP*s, and the modal, median and mean effective radii as a function of *LWP* for the northernmost (5–10°N) and the southernmost (5–10°S) regions. These two regions contain more data points than the other two regions. The results are shown in Figures 11 and 12. There is a clear difference in frequency distributions of effective radius between the two regions (Figure 11). That is, given a fixed value of *LWP*, clouds in the south tend to have larger effective radii than clouds in the north. This difference is also shown in modal, median, and mean radii plots (Figure 12), particularly for clouds in the large *LWP* range. The biggest difference is shown in the modal radius while the mean radius shows smaller differences. This result is an indication that high aerosol concentration in the north has reduced the cloud droplet size by increasing number concentration of cloud droplets. For small *LWP* (e.g.,

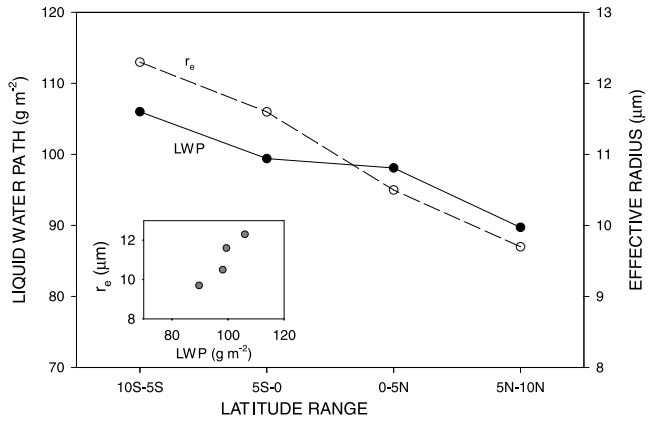

Figure 9. Latitudinal distribution of liquid water path and effective radius averaged in each 5° latitudinal region. Inset: Scatterplot of the averaged liquid water path and effective radius.

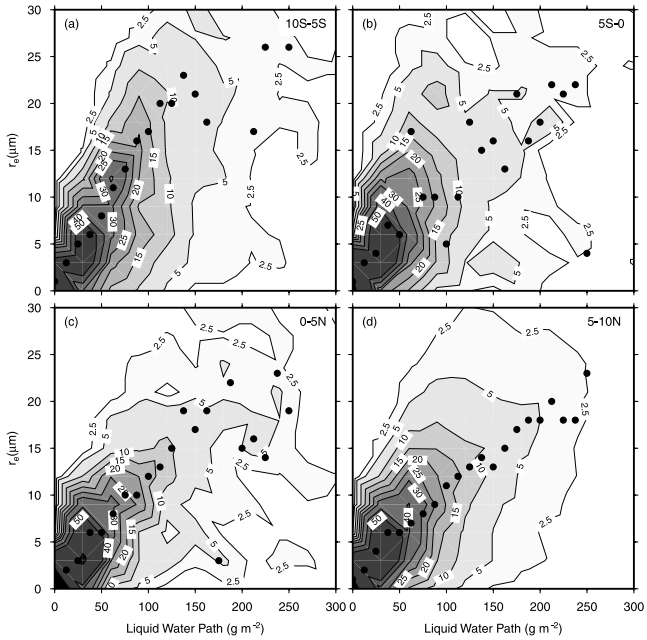

Figure 10. Frequency distribution of pixel occurrence in the two-dimensional diagram of liquid water path and effective radius for the following four latitudinal regions. (a) 5–10°S, (b) 0–5°S, (c) 0–5°N, and (d) 5–10°N. Solid dots show the modal effective radii at fixed liquid water path.

LWP = 25 g m^{-2}), the difference in the effective radius between the two regions is less clear. Although the small difference may be a true reflection of the real clouds, the large uncertainty in the effective radius retrieval in the small *LWP* range (c.f. Figure 4) makes it difficult to draw a reliable conclusion.

4.3. North-South Gradient of Cloud Droplets Concentration From In Situ Data

[27] As mentioned in the introduction, the INDOEX region is characterized by strong north-south gradient of anthropogenic aerosols as a result of the polluted airmass over the Indian subcontinent and the clean airmass over tropical oceans. The difference in *LWP*-r_e relations described earlier suggests that clouds in the INDOEX domain have responded to this aerosol gradient, that is, smaller cloud radii to the north and larger cloud radii to the south, given the same values of *LWP*. To further elaborate this point, we analyze the in situ data of cloud drop concentrations measured by FSSP-100 on C-130 aircraft. Within every 1° (latitude) by 1° (longitude) box, we average the highest 10 values registered on FSSP-100s one-second number concentration data during any of the 18 flights. The highest values are used on the assumption that they arise from measurements well within a cloud where cloud water has not been diluted by surrounding drier air. Figure 13 shows the distribution of the averaged values of the FSSP-100 cloud drop number concentration. The highest concentration was observed near the northeast corner of the region with a value of $\sim$ 500 cm^{-3}. The concentration decreases toward the south to $\sim$ 100 cm^{-3} at the southernmost extent of the region. Again, this diagram suggests that the aerosol concentration is affecting the number concentration of cloud droplets in the INDOEX domain, which is consistent with our results based on *LWP* and r_e retrievals.

[28] Using the in situ aircraft cloud drop number concentration and retrievals of liquid water path and effective radius, we estimated the magnitude of terms shown in (2) by taking the differences of *LWP*, r_e and N_c between northern and southern hemispheres. The relative difference in cloud number concentration estimated from data in Figure 13 is $\Delta N_c/N_c \sim 0.6$. From data shown in Figure 9, the relative differences in effective radius and liquid water path were estimated as $3\Delta r_e/r_e \sim -0.5$ and $\Delta LWP/LWP \sim -0.1$. Consequently, it appears that the increase in cloud droplet number concentration from southern to northern hemispheres is roughly balanced by the decrease in effective radius of cloud droplets while leaving the liquid water contents approximately the same. Similar findings were reported by *Heymsfield and McFarquar* [2001] based solely on in situ aircraft microphysical observations. Additionally, the $\sim$10% difference in liquid water path together with the $\sim$10% imbalance between $\Delta N_c/N_c$ and $3\Delta r_e/r_e$ suggests that the average cloud thickness in the northern hemisphere is $\sim$20% smaller than that in the southern hemisphere. This

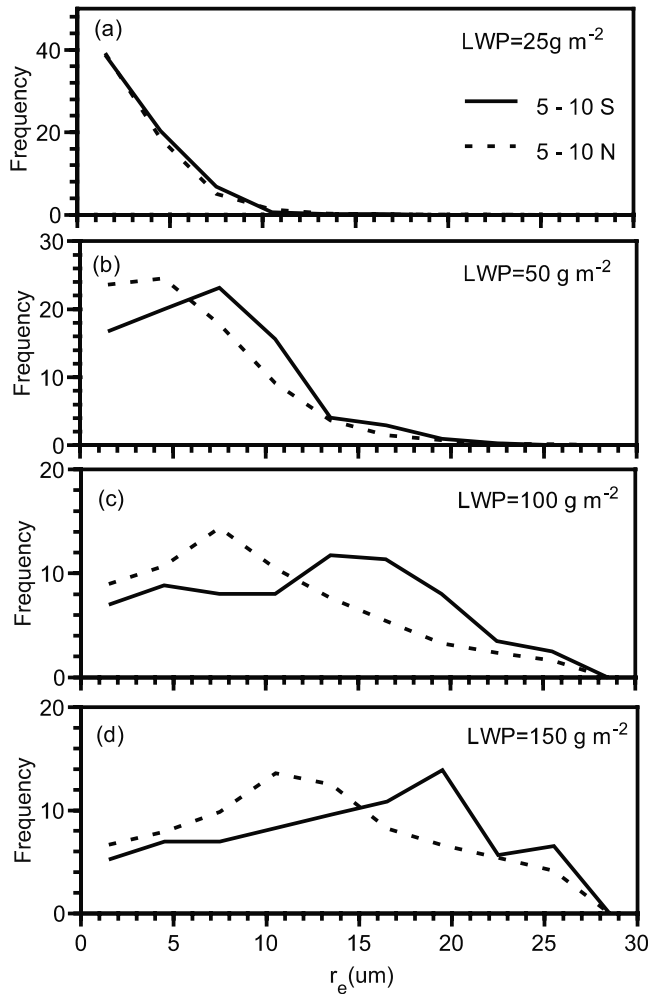

Figure 11. Comparison of frequency distributions of effective radius at liquid water path of (a) 25 g m^{-2}, (b) 50 g m^{-2}, (c) 100 g m^{-2}, and (d) 150 g m^{-2} between 5–10°S and 5–10°N regions.

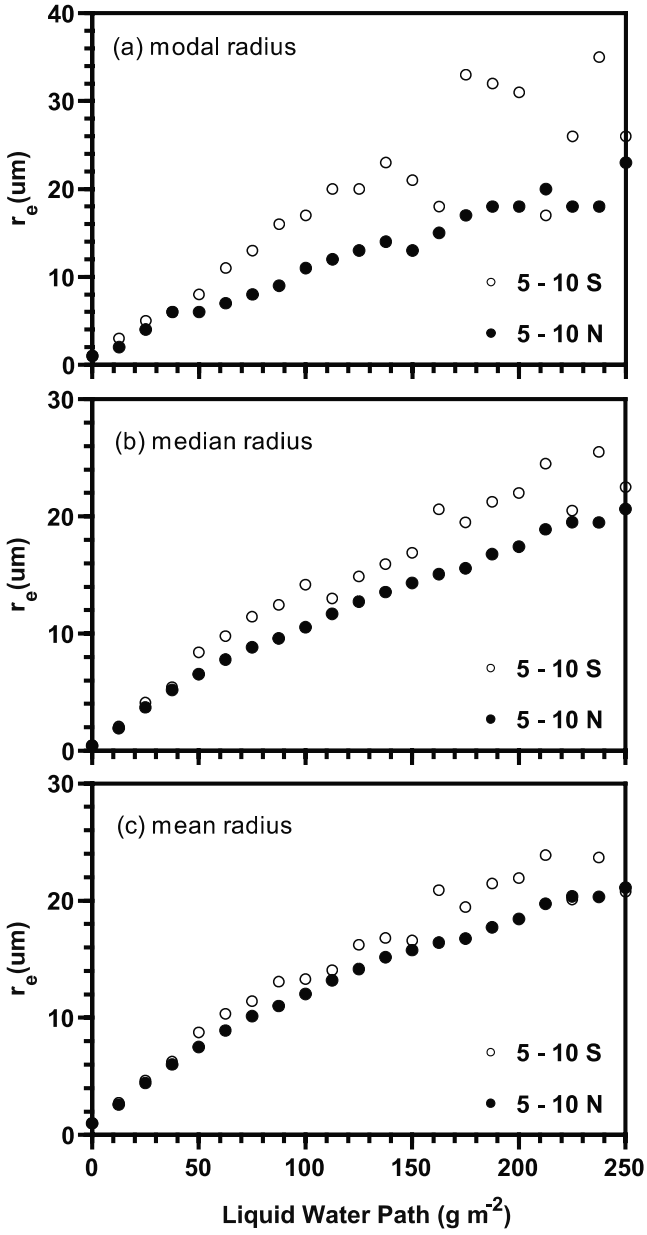

Figure 12. Relations between liquid water path and (a) modal radius, (b) median radius, and (c) mean radius for the southern (5–10°S) and northern (5–10°N) regions.

difference may be a reflection of the differences in atmospheric thermodynamical structures between the two hemispheres and/or due to aerosols' cloud thinning effect as suggested by *Ackerman et al.* [2000].

5. Conclusions

[29] The effective radius of water cloud droplets was retrieved using remotely sensed microwave and visible data collected by airborne radiometers during the INDOEX experiment. The INDOEX domain is characterized by a strong north-south gradient of aerosol concentration due to the contrast of the polluted airmass from Indian subcontinent and the clean airmass in the ITCZ. This study aims to assess whether the aerosol concentration gradient gives rise to the difference in effective radii of cloud droplets between the northern and southern regions.

[30] The effective radius is retrieved from the reflectance at 0.64 μm and liquid water path derived from microwave observations. Error analysis using a Monte Carlo procedure shows that the largest error occurs for thin clouds having small 0.64 μm reflectances and small liquid water paths. For this reason, only pixels with a reflectance larger than 0.2 are used in the data analysis, which limits the maximum RMS error in effective radius to about 4 μm. To minimize the error caused by horizontal inhomogeneity of cloud field, we excluded the cloudy scenes that only have clouds less than 2 km in horizontal scale.

[31] Thirty-five cloudy scenes were selected for this study, which were located approximately along 70°E from 10°S to 10°N. The averaged liquid water path and effective radius both show north-south gradients with higher values in the southern regions. We first investigated two cases, one in clean air and the other in polluted air. For the same value of liquid water path, effective radii are smaller in the polluted case than in the clean case. Investigation for four latitudinal regions shows that for the same liquid water path, effective radii are significantly smaller in the northern regions than in the southern regions, corresponding to the aerosols' north-south gradient. In situ aircraft measurement by FSSP-100 also shows the north-south gradient of cloud droplet number concentration. The north-south differences in liquid water path, effective radius, and cloud number concentration are consistent with the hypothesis of the aerosols' effect on cloud microphysics, that is, higher aerosol concentration increases the number concentration of cloud droplets, which in turn reduces droplet sizes given the same liquid water path and cloud thickness. Furthermore, a rough estimate of the differences in effective radii and cloud number concentrations between the two hemi-

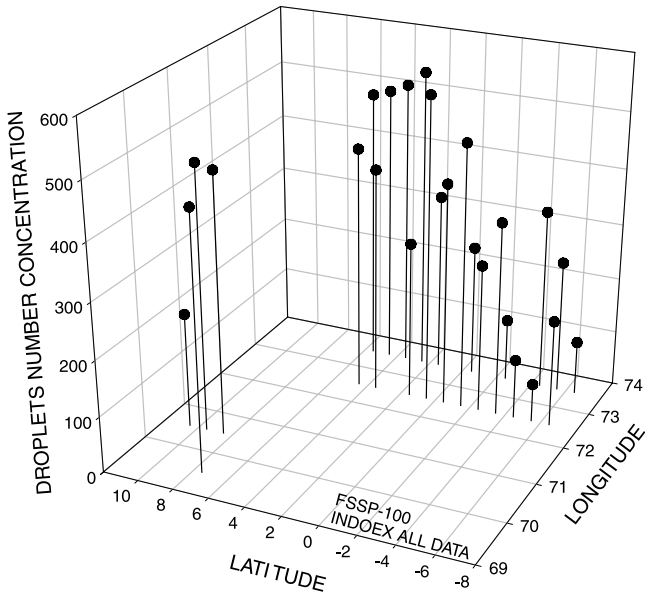

Figure 13. Distribution of particle number concentration measured by FSSP-100. The number concentration shown here is the average of the highest 10 values in each 1° × 1° grid observed during INDOEX experiment.

spheres suggests that the aerosol number concentration alters cloud droplet numbers and sizes while leaving liquid water contents approximately the same. Due to the limitation of aircraft measurements, further research efforts using satellite observations are needed to extend the investigation to global and long timescales. Additionally, collecting ground truth data in future field experiments will be very valuable to validate liquid water path and effective radius retrievals.

[32] **Acknowledgments.** We thank scientists and engineers at NCAR, especially Craig Walther and Krista Laursen, for collecting the AIMR and MCR data during INDOEX and processing them after the experiment. Comments and suggestions from Qingyuan Han at the University of Alabama in Huntsville and two anonymous reviewers were very helpful. This research has been supported by NSF Grant ATM-0002860 and NASA Grant NAG5-8647. J. Curry's participation was supported by the NASA FIRE project. J. Coakley's participation was supported by NSF through the Center for Clouds, Chemistry, and Climate (C^4), a national science and technology center at the Scripps Institution of Oceanography and by NSF Grant ATM-9612886.

References

Ackerman, A. S., O. B. Toon, D. E. Stevens, A. J. Heymsfield, V. Ramanathan, and E. J. Welton, Reduction of tropical cloudiness by soot, *Science*, *288*, 1042–1047, 2000.

Brenguier, J.-L., H. Pawlowska, L. Schuller, R. Preusker, J. Fischer, and Y. Fouquart, Radiative properties of boundary layer clouds: Droplet effective radius versus number concentration, *J. Atmos. Sci.*, *57*, 803–821, 2000.

Coakley, J. A., Jr., R. L. Bernstein, and P. A. Durkee, et al., Effect of ship-track effluents on cloud reflectivity, *Science*, *237*, 1020–1022, 1987.

Collins, M. J., F. G. R. Warren, and J. L. Paul, Airborne imaging microwave radiometer - Part I: Radiometric analysis, *IEEE Trans. Geosci. Remote Sens.*, *34*, 643–655, 1996.

Curran, R. J., H. L. Kyle, L. R. Blaine, J. Smith, and T. D. Clem, Multichannel scanning radiometer for remote sensing cloud physical parameters, *Rev. Sci. Instrum.*, *52*, 1546–1555, 1981.

Dye, J. E., and D. Baumgardner, Evaluation of the forward scattering spectrometer probe Part I: Electronic and optical studies, *J. Atmos. Oceanic. Technol.*, *1*, 330–344, 1984.

Greenwald, T. J., G. L. Stephens, S. A. Christopher, and T. H. Vonder Haar, Observations of the global characteristics and regional radiative effects of marine cloud liquid water, *J. Clim.*, *8*, 2928–2946, 1995.

Han, Q., W. B. Rossow, and A. A. Lacis, Near-global survey of effective droplet radii in liquid water cloud using ISCCP data, *J. Clim.*, *7*, 465–497, 1994.

Han, Q., W. B. Rossow, J. Chou, and R. M. Welch, Global survey of the relationships of cloud albedo and liquid water path with droplet size using ISCCP, *J. Clim.*, *11*, 1516–1528, 1998.

Heymsfield, A. J., and G. M. McFarquhar, Microphysics of INDOEX clean and polluted trade cumulus clouds, *J. Geophys. Res.*, *106*, 28,653–28,674, 2001.

Jayaraman, A., D. Lubin, S. Ramachandran, V. Ramanathan, E. Woodbridge, W. Collins, and K. S. Zalpuri, Direct observations of aerosol radiative forcing over the tropical Indian Ocean during the Jan.-Feb.-1996 Pre-INDOEX cruise, *J. Geophys. Res.*, *103*, 13,827–13,836, 1998.

Lin, B., B. Wielicki, P. Minnis, and W. B. Rossow, Estimation of water cloud properties from satellite microwave, infrared and visible measurements in oceanic environments, 1, Microwave brightness temperature simulations, *J. Geophys. Res*, *103*, 3873–3886, 1998a.

Lin, B., P. Minnis, B. Wielicki, D. R. Doelling, R. Palikonda, D. F. Young, and T. Uttal, Estimation of water cloud properties from satellite microwave, infrared and visible measurements in oceanic environments, 2, Results, *J. Geophys. Res.*, *103*, 3887–3905, 1998b.

Liu, G., and J. A. Curry, Determination of ice water path and mass median particle size using multichannel microwave measurements, *J. Appl. Meteorol.*, *39*, 1318–1329, 2000.

Liu, G, J. A. Curry, J. A. Haggerty, and Y. Fu, Retrieval and characterization of cloud liquid water path using airborne passive microwave data during INDOEX, *J. Geophys. Res.*, *106*, 28,719–28,730, 2001.

Masunaga, H., T. Y. Nakajima, T. Nakajima, M. Kachi, R. Oki, and S. Kuroda, Physical properties of maritime low clouds as retrieved by combined use of Tropical Rainfall Measurement Mission Microwave Imager and Visible/Infrared Scanner: Algorithm, *J. Geophys. Res.*, *107*, 4083, doi:10.1029/2001JD000743, 2002.

McClatchey, R. A., R. W. Fenn, J. E. A. Selby, F. E. Volz, and J. S. Garing, Optical properties of the atmosphere, 3rd ed., *AFCRL Environ. Res.Papers No. 411*, 108 pp., 1972.

Minnis, P., P. W. Heck, D. F. Young, C. W. Fairall, and J. B. Snider, Stratocumulus cloud properties derived from simultaneous satellite and island-based instrumentation during FIRE, *J. Appl. Meteorol.*, *31*, 317–339, 1992.

Nakajima, T., and M. D. King, Determination of the optical thickness and effective particle radius of clouds from reflected solar radiation measurements, Part I, Theory, *J. Atmos. Sci.*, *47*, 1878–1893, 1990.

Nakajima, T., M. D. King, and J. D. Spinhirne, Determination of the optical thickness and effective particle radius of clouds from reflected solar radiation measurements, Part II, Marine stratocumulus observations, *J. Atmos. Sci.*, *48*, 728–750, 1991.

Nakajima, T., A. Higurashi, K. Kawamoto, and J. E. Penner, A possible correlation between satellite-derived cloud and aerosol microphysical parameters, *Geophys. Res. Lett.*, *78*, 1171–1174, 2001.

Radke, L. F., J. A. Coakley Jr., and M. D. King, Direct and remote sensing observations of the effects of ships on clouds, *Science*, *246*, 1146–1149, 1989.

Ramanathan, V., P. J. Crutzen, J. T. Kiehl, and D. Rosenfeld, Aerosols, climate, and the hydrological cycle, *Science*, *294*, 2119–2124, 2001a.

Ramanathan, V., et al., Indian Ocean Experiment: An integrated assessment of climate forcing and effects of the great Indo-Asian haze, *J. Geophys. Res.*, *106*, 28,371–28,398, 2001b.

Rhoads, K., P. Keley, R. Dickerson, T. Carsey, M. Farmer, D. Savoi, and J. Propero, The composition of the troposphere over the Indian Ocean during the monsoonal transition, *J. Geophys. Res.*, *102*, 18,981–18,995, 1997.

Ricchiazzi, P., S. Yang, C. Gautier, and D. Sowle, SBDART: A research and teaching software tool for plane-parallel radiative transfer in the Earth's atmosphere, *Bull. Am. Meteorol. Soc.*, *79*, 2101–2114, 1998.

Stamnes, K., S. Tsay, W. Wiscombe, and K. Jayaweera, Numerically stable algorithm for discrete-ordinate-method radiative transfer in multiple scattering and emitting layered media, *Appl. Opt.*, *27*, 2502–2509, 1988.

Szczodrak, M., P. H. Austin, and P. B. Krummel, Variability of optical depth and effective radius in marine stratocumulus clouds, *J. Atmos. Sci.*, *58*, 2912–2926, 2001.

Tanre, D., C. Deroo, P. Duhaut, M. Herman, J. J. Morcrette, J. Perbos, and P. Y. Deschamps, Description of a computer code to simulate the satellite signal in the solar spectrum: The 5S code, *Int. J. Remote Sens.*, *11*, 659–668, 1990.

Tschudi, M. A., and K. K. Laursen, Airborne spectral reflectance observations at SHEBA from NCAR's Multichannel Cloud Radiometer (MCR), Paper presented at the Sixth Conference on Polar Met and Oceanography, Am. Meteorol. Soc., San Diego, Calif., 147–150, 2001.

Twomey, S., M. Piepgrass, and T. L. Wolfe, An assessment of the impact of pollution on global cloud albedo, *Tellus*, *36B*, 356–366, 1984.

Zuidema, P., and D. L. Hartmann, Satellite determination of stratus cloud microphysical properties, *J. Clim.*, *8*, 1638–1657, 1995.

J. A. Coakley Jr., College of Oceanic and Atmospheric Sciences, Oregon State University, Corvallis, OR 97331, USA. (coakley@oce.orst.edu)

J. A. Curry, Program in Atmospheric and Oceanic Sciences, University of Colorado, Campus Box 429, Boulder, CO 80309, USA. (curryja@cloud.colorado.edu)

G. Liu and H. Shao, Department of Meteorology, Florida State University, 404 Love Building, Tallahassee, FL 30306-4520, USA. (liug@met.fsu.edu; soar@met.fsu.edu)

J. A. Haggerty and M. A. Tschudi, Atmospheric Technology Division, National Center for Atmospheric Research, Boulder, CO 80307, USA. (julie@raf.atd.ucar.edu; tschudi@ucar.edu)